II ECCOMAS Thematic Conference on Smart Structures and Materials

Paper

Design by: Ana Espada & Leonardo Rosado :: lhr@netcabo.pt

Instituto Superior Técnico, Lisbon 18 / 21 July 2005

FUNDAÇÃO CALOUSTE GULBENKIAN

FCT Fundação para a Ciência e a Tecnologia
MINISTÉRIO DA CIÊNCIA, TECNOLOGIA E ENSINO SUPERIOR

APMTAC

II ECCOMAS THEMATIC CONFERENCE ON SMART STRUCTURES AND MATERIALS
C.A. Mota Soares *et al.* (Eds.)
Lisbon, Portugal, July 18 - 21, 2005

COMBINED FEEDBACK/FEEDFORWARD ACTIVE CONTROL OF VIBRATION OF BEAMS WITH ACLD TREATMENTS: NUMERICAL SIMULATION

César M. A. Vasques and José D. Rodrigues

Departamento de Engenharia Mecânica e Gestão Industrial
Faculdade de Engenharia da Universidade do Porto
Rua Dr. Roberto Frias s/n, 4200-465 Porto, Portugal
e-mail: cvasques@fe.up.pt and jdr@fe.up.pt

Keywords: Adaptive beam, PCLD, ACLD, vibration, control, feedback, feedforward.

Abstract. *This paper concerns the numerical simulation of feedback, adaptive feedforward and combined feedback/feedforward control systems on the active control of vibrations of beams with active constrained layer damping (ACLD) treatments. For the simulation a 1-D finite element (FE) model of beams with an arbitrary number of elastic, piezoelectric and viscoelastic layers attached to both sides of the beam is utilized. The damping behavior of the viscoelastic layers is considered by a Laplace transformed Anelastic Displacement Fields (ADF) method. The simulation is performed using Matlab® and Simulink® softwares. The analyzed case study regards the disturbance rejection of an aluminium beam with a pair of surface mounted ACLD patches. In the design and simulation of the control system a single-input single-output (SISO) configuration with the output being the velocity at one point of the beam and the input being the control voltage applied into the piezoelectric constraining layers is considered. The case study allows to assess and discuss the outcomes and drawbacks of the feedback and feedforward controllers when used individually and the advantages of the hybrid controller.*

1 INTRODUCTION

Active constrained layer damping (ACLD) treatments have revealed from the early 1990s to be an effective means of vibration suppression [1]. In an attempt to improve performance different configurations of the constraining active piezoelectric and passive viscoelastic layers have been used. These treatments are called arbitrary ACLD treatments or hybrid active-passive damping treatments. The ACLD treatments combine the high passive capacity of viscoelastic materials to dissipate vibrational energy at high frequencies with the active capacity of piezoelectric materials at low frequencies. Therefore, in the same damping treatment, a broader band control is achieved benefiting from the advantages of both passive (simplicity, stability, fail-safe, low-cost) and active (adaptability, high-performance) systems. A survey of advances in hybrid

active-passive vibrations and noise control via piezoelectric and viscoelastic constrained layer treatments can be found in references [2–4].

In the last decades the advances in digital signal processing and sensors and actuators technology have prompted interest in active control and a considerable effort has been put in the development and implementation of active noise and vibration control theories (see related textbooks [5–9]). These might be divided into two fundamental classes, namely, feedback and feedforward control algorithms. The former control strategy has been shown to be most suitable in applications where the structure is under impulsive or stochastic unknown disturbances and the latter to the case where deterministic or correlated information about the disturbance is known. A review paper concerning active structural vibration control is presented in reference [10].

In the open literature several works can be found where feedback theories are applied in vibration control of beams with arbitrary ACLD (hybrid active-passive) treatments. However, only a few works utilizing feedforward theory can be found [11, 12]. The most typical application of feedforward control presented in textbooks concerns the noise attenuation in ducts and applications concerning vibration reduction are mainly devoted to active structural acoustic control (ASAC). To the knowledge of the authors the use of hybrid (combined feedback/feedforward) control is in this work analyzed for the first time for structural systems with this kind of damping treatment.

This paper concerns the numerical simulation of feedback, adaptive feedforward and a combined feedback/feedforward control systems on the active control of vibrations of beams with ACLD treatments. First a 1-D finite element (FE) model of beams with an arbitrary number of elastic, piezoelectric and viscoelastic layers attached to both sides of the beam [13, 14], which will be utilized in the simulation and design, is succinctly presented. Next, the damping behavior of the viscoelastic layers is considered by a Laplace transformed *Anelastic Displacement Fields* (ADF) method and its FE model implementation is presented. Then, for the design of the control system architecture, the optimal feedback *Linear Quadratic Gaussian* (LQG) and feedforward *filtered-reference LMS* controllers are presented and discussed when utilized in a unified way (hybrid controller). Finally, a case study regarding the disturbance rejection of an aluminium beam with a pair of symmetrically collocated surface mounted ACLD patches is analyzed with the simulation being performed with Matlab® and Simulink® software. In the design and simulation of the control system a single-input single-output (SISO) configuration with the output being the velocity at one point of the beam and the input being the control voltage applied into the piezoelectric constraining layers is considered. First a broadband stochastic disturbance is considered and the feedback controller is utilized to suppress vibration. Then, considering that the designer has access to a periodic reference signal that is correlated with the disturbance, an adaptive feedforward strategy is employed to cancel the effects of the disturbance on the system at the chosen output location. Finally, both controllers are combined into a unified hybrid controller.

2 BEAMS WITH ARBITRARY ACLD TREATMENTS

When designing hybrid active-passive treatments it is important to know the configuration of the structure and treatment that gives optimal damping. For simulation the designer needs a model of the system in order to define the optimal locations, thicknesses, configurations, control law, etc. Thus, there are numerous options at the design stage. The task of modeling beams with arbitrary ACLD treatments often requires the development of a coupled model of the structure, which comprises piezoelectric, viscoelastic and elastic layers. In the development of FE models different assumptions can be taken into account in the theoretical model when considering the mechanical model, the damping introduced by the viscoelastic materials and the electro-mechanical coupling. The mechanical model assumptions concern the definition of the displacement field. The electro-mechanical ones regard mainly the use (or not) of electric degrees of freedom (DoFs) and the approximations of the through-the-thickness variation of the electric potential. Therefore, they lead to decoupled, partial and fully coupled electro-mechanical theories, which in turn can lead to different modifications of the structure's stiffness and different approximations of the physics of the system. Furthermore, different damping models in the frequency or time domain may be utilized to characterize the damping behavior of the viscoelastic materials.

2.1 Finite Element Model

In this section the FE model of a beam with arbitrary ACLD treatments is presented. For the sake of brevity the reader is referred to the works of Vasques *et al.* [13, 14] for further details.

Consider the layered beam illustrated in Figure 1. The composite beam consists of a host beam, layer 0, of thickness $2h_0$, to which other layers (treatments) are attached. In order to be able to model several configurations of the treatments, the composite beam theory allows an arbitrary number of layers of elastic, piezoelectric and viscoelastic materials in arbitrary positions. There are $\bar{n}$ layers on the top surface and $-\bar{m}$ layers on the bottom surface. The displacement field is defined according to a partial layerwise theory where the axial and transverse displacements, $\tilde{u}_k(x, z_k, t)$ and $\tilde{w}_k(x, t)$, of the top ($n = 1, \ldots, \bar{n}$), core ($c = 0$) and bottom ($m = \bar{m}, \ldots, -1$) layers are given by

$$\tilde{u}_n(x, z_n, t) = u_0(x, t) + h_0\theta_0(x, t) + \sum_{i=1}^{n-1} 2h_i\theta_i(x, t) + (z_n + h_n)\theta_n(x, t), \tag{1a}$$

$$\tilde{u}_c(x, z_c, t) = u_0(x, t) + z_0\theta_0(x, t), \tag{1b}$$

$$\tilde{u}_m(x, z_m, t) = u_0(x, t) - h_0\theta_0(x, t) - \sum_{i=m+1}^{-1} 2h_i\theta_i(x, t) + (z_m - h_m)\theta_m(x, t), \tag{1c}$$

$$\tilde{w}_k(x, t) = \tilde{w}_n(x, t) = \tilde{w}_c(x, t) = \tilde{w}_m(x, t) = w_0(x, t), \tag{1d}$$

where $2h_k$ is the thickness of the kth layer ($k = \bar{m}, \ldots, -1, 0, 1, \ldots, \bar{n}$), $u_0(x, t)$, $w_0(x, t)$ and $\theta_0(x, t)$ are, respectively, the generalized axial and transverse displacements and the rotation of the beam's mid-plane, and $\theta_n(x, t)$ and $\theta_m(x, t)$ are the rotation of each nth top and mth bottom layer. Furthermore, axial displacement continuity at the interfaces of the layers is assured,

leading to coupling terms in the axial displacements of the layers, and a constant through-the-thickness transverse displacement $w_0(x,t)$ is considered.

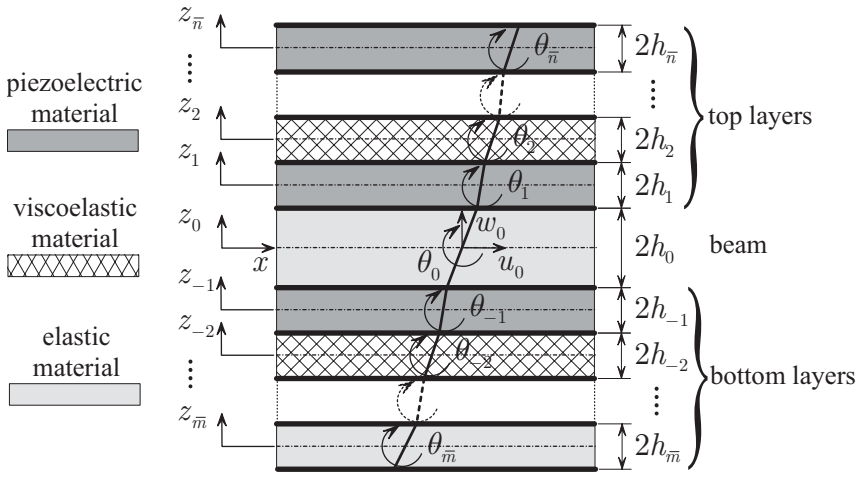

Figure 1. Partial layerwise displacement field of the beam with an arbitrary ACLD treatment.

The material of the piezoelectric layers is assumed to be orthotropic with the symmetry properties of an orthorhombic crystal of the class $mm2$ [15, 16]. In the present work, a fully coupled electro-mechanical theory which takes into account the direct piezoelectric effect with a non-linear distribution of the electric potential is utilized and the direct piezoelectric effect is considered by the use of *effective stiffness parameters* [17, 18], which should be defined according to the electric boundary condition considered.

The weak forms governing the motion and electric charge equilibrium of the layered beam with arbitrary ACLD treatments (elastic, piezoelectric and viscoelastic layers located in arbitrary positions in the laminate) are obtained from Hamilton's principle where the Lagrangian and the work of the externally applied forces are adapted for the electrical and mechanical contributions [19], so that

$$\delta \int_{t_0}^{t_1} (T - H + W)\, \mathrm{d}t = 0, \tag{2}$$

where t_0 and t_1 define the time interval, δ denotes the variation, T is the kinetic energy, H is the electro-mechanical enthalpy (energy stored in the piezoelectric and non-piezoelectric layers) and W denotes the work done by the externally applied mechanical forces and electrical charges. In the resultant weak forms the generalized displacements and electrical potential differences vectors are the unknown independent variables.

The FE method is utilized to discretize the weak forms and the generalized displacements within each element domain are approximated by linear C^0 interpolation functions [20] and constant functions are utilized to approximate the electric potential differences. As a consequence, the electric potential difference becomes constant in each element. The FE mesh is

then composed of $q+1$ nodal points and the global mechanical and electrical degrees of freedom (DoFs) vectors, $\bar{\mathbf{u}}(t)$ and $\bar{\boldsymbol{\phi}}(t)$, are defined as

$$\bar{\mathbf{u}}(t) = \left\{\ldots, \bar{u}_0^r(t), \bar{w}_0^r(t), \bar{\theta}_0^r(t), \bar{\theta}_1^r(t), \cdots, \bar{\theta}_{\bar{n}}^r(t), \bar{\theta}_{\bar{m}}^r(t), \cdots, \bar{\theta}_{-1}^r(t), \ldots\right\}^{\mathrm{T}}, \tag{3}$$

$$\bar{\boldsymbol{\phi}}(t) = \left\{\ldots, \bar{\phi}_1^s(t), \cdots, \bar{\phi}_{\bar{n}}^s(t), \bar{\phi}_{\bar{m}}^s(t), \cdots, \bar{\phi}_{-1}^s(t), \ldots\right\}^{\mathrm{T}}, \tag{4}$$

where $r = 1, \ldots, q+1$ and $s = 1, \ldots, q$. The superscript r denotes the node at which the DoF is defined and the subscript identifies the layer to which the DoF refers.

The global equations of motion and charge equilibrium of the discrete system are given by

$$\mathbf{M}_{uu}\ddot{\bar{\mathbf{u}}}(t) + \mathbf{K}_{uu}\bar{\mathbf{u}}(t) + \mathbf{K}_{\phi u}^{\mathrm{T}}\bar{\boldsymbol{\phi}}(t) = \mathbf{F}_u(t), \tag{5a}$$

$$\mathbf{K}_{\phi u}\bar{\mathbf{u}}(t) + \mathbf{K}_{\phi\phi}\bar{\boldsymbol{\phi}}(t) = \mathbf{Q}(t), \tag{5b}$$

where $\mathbf{M}_{uu}$ and $\mathbf{K}_{uu}$ are the global mass and stiffness matrices, $\mathbf{K}_{u\phi} = \mathbf{K}_{\phi u}^{\mathrm{T}}$ is the global piezoelectric coupling matrix, $\mathbf{K}_{\phi\phi}$ is the global capacitance matrix and $\mathbf{F}_u(t)$ and $\mathbf{Q}(t)$ are the global mechanical force and electric charge vectors (see [13, 14] for further details).

The electrical DoFs vector in Equations (5) can be partitioned into the actuating and sensing DoFs, $\bar{\boldsymbol{\phi}}(t) = \mathrm{col}[\bar{\boldsymbol{\phi}}_{\mathrm{a}}(t), \bar{\boldsymbol{\phi}}_{\mathrm{s}}(t)]$, where the subscripts $(\cdot)_{\mathrm{a}}$ and $(\cdot)_{\mathrm{s}}$ denote the actuating and sensing capabilities. Furthermore, the stiffness matrix can be written as the sum of the elastic and piezoelectric layers stiffness matrices $\mathbf{K}_{uu}^E$ and $\mathbf{K}_{uu}^P$. Hence, considering open-circuit electrodes, and in that case $\mathbf{Q}(t) = 0$ [18], the non specified potential differences in (5b) can be statically condensed in (5a) and the equations of motion and charge equilibrium become

$$\mathbf{M}_{uu}\ddot{\bar{\mathbf{u}}}(t) + \left(\mathbf{K}_{uu}^E + \mathbf{K}_{uu}^{P*}\right)\bar{\mathbf{u}}(t) = -\mathbf{K}_{\phi u\mathrm{a}}^{\mathrm{T}}\bar{\boldsymbol{\phi}}_{\mathrm{a}}(t) + \mathbf{F}_u(t), \tag{6a}$$

$$\bar{\boldsymbol{\phi}}_{\mathrm{s}}(t) = -\mathbf{K}_{\phi\phi\mathrm{s}}^{-1}\mathbf{K}_{\phi u\mathrm{s}}\bar{\mathbf{u}}(t), \tag{6b}$$

where

$$\mathbf{K}_{uu}^{P*} = \mathbf{K}_{uu}^P - \mathbf{K}_{\phi u\mathrm{s}}^{\mathrm{T}}\mathbf{K}_{\phi\phi\mathrm{s}}^{-1}\mathbf{K}_{\phi u\mathrm{s}}.$$

It's worthy to mention that a through-the-thickness parabolic distribution of the electric potential within the piezoelectric layers was already considered in the variational formulation through the use of effective stiffness parameters and therefore the static condensation in Equation (6a) only considers the linear counterpart of the electrical potential distribution, which is the one that in fact contributes to the sensor voltage. Moreover, a second alternative where the equipotential area condition is satisfied by means of a modified static condensation of the non-specified potentials might be utilized, which corresponds to a more realistic approach, that becomes more significant for bare piezoelectric beams or as the length of the piezoelectric layers approaches the length of the host beam (see [18, 21] for further details).

2.2 Viscoelastic Damping Model

The temperature and frequency dependent material properties of the viscoelastic materials causes some difficulties for the mathematical model, increasing its complexity. Usually the temperature is assumed constant and only models concerning frequency dependence are utilized. A time domain model such as the *Anelastic Displacement Fields* (ADF) [22, 23] is utilized in this

work and represents a good alternative to frequency domain methods for the study of transient responses.

Assuming a constant operating temperature (isothermal condition) and simple harmonic excitation, the constitutive behavior of the viscoelastic materials can be characterized in the frequency domain by a complex shear or extensional modulus, $G\left(j\omega\right)$ or $E\left(j\omega\right)$, and a loss factor $\eta\left(\omega\right)$, which accounts for energy dissipation effects [24–26]. Considering this constitutive behavior the FE equation of motion in (6a) can be written as

$$\mathbf{M}_{uu}\ddot{\bar{\mathbf{u}}}(t)+\Big(\mathbf{K}_{uu}^{E}+\mathbf{K}_{uu}^{P*}+\mathbf{K}_{uu}^{V}(j\omega)\Big)\bar{\mathbf{u}}(t)=-\mathbf{K}_{u\phi\mathrm{a}}\bar{\boldsymbol{\phi}}_{\mathrm{a}}(t)+\mathbf{F}_{u}(t), \tag{7}$$

where $\mathbf{K}_{uu}^{V}(j\omega)$ is the complex frequency dependent global stiffness matrix of the viscoelastic layers.

In the ADF model developed by Lesieutre [22, 23] the self-heating effects of the viscoelastic layers are neglected, and only the frequency dependence of the viscoelastic material is taken into account. Thus, the complex shear modulus of the viscoelastic layers, originally formulated in the frequency domain by Lesieutre [22, 27], may be represented by a series of functions in the Laplace domain, such that

$$G(s)=G_{0}\Big(1+\sum_{i=1}^{n}\frac{\Delta_{i}s}{s+\Omega_{i}}\Big), \tag{8}$$

where $G_0=\lim_{t\to\infty}G(t)$ is the is the relaxed (or static) shear modulus, Ω_i is the inverse of the characteristic relaxation time at constant strain and Δ_i the correspondent relaxation resistance. The relaxed shear modulus G_0 and the series of material parameters Δ_i and Ω_i are evaluated by curve fitting of the measurements of $G(j\omega)$.

Considering the stiffness matrices of the non-viscoelastic layers, $\mathbf{K}_{uu}^{EP*}=\mathbf{K}_{uu}^{E}+\mathbf{K}_{uu}^{P*}$, and the total force vector given by the sum of the mechanical and electrical loads, $\mathbf{F}(t)=\mathbf{F}_{u}(t)+\mathbf{F}_{\phi}(t)$, with $\mathbf{F}_{\phi}(t)=-\mathbf{K}_{u\phi\mathrm{a}}\bar{\boldsymbol{\phi}}_{\mathrm{a}}(t)$, if we now write the Laplace transform of Equation (7) yields

$$\Big(s^{2}\mathbf{M}_{uu}+s\mathbf{D}_{uu}+\mathbf{K}_{uu}^{EP*}+G(s)\bar{\mathbf{K}}_{uu}^{V}\Big)\tilde{\mathbf{u}}(s)=\tilde{\mathbf{F}}(s)+\mathbf{M}_{uu}\Big(\dot{\bar{\mathbf{u}}}_{0}+s\bar{\mathbf{u}}_{0}\Big)+\mathbf{D}_{uu}\bar{\mathbf{u}}_{0}, \tag{9}$$

where $\tilde{\mathbf{u}}(s)$ and $\tilde{\mathbf{F}}(s)$ are the Laplace transforms of the displacement and summed mechanical and electrical force vectors, $\bar{\mathbf{u}}_0$ and $\dot{\bar{\mathbf{u}}}_0$ are the initial displacement and velocity vectors, and the stiffness matrix of the viscoelastic layers was expressed as $\mathbf{K}_{uu}^{V}(s)=G(s)\bar{\mathbf{K}}_{uu}^{V}$ (both shear and extensional stiffness terms were considered in $\bar{\mathbf{K}}_{uu}^{V}$ through the extensional and shear modulus relationship). Furthermore, a viscous proportional damping model matrix $\mathbf{D}_{uu}$ is considered in the previous equation to model the material damping of the beam and non-viscoelastic layers.

The ADF model is based in a separation of the viscoelastic material strains in an elastic part, instantaneously proportional to the stress, and an anelastic part representing material relaxation. Its implementation on a FE model [28, 29] consists of replacing the DoFs of the vector $\tilde{\mathbf{u}}(s)$, which are associated with the viscoelastic layers strain energy, by

$$\tilde{\mathbf{u}}(s)=\tilde{\mathbf{u}}^{E}(s)+\sum_{i=1}^{n}\tilde{\mathbf{u}}_{i}^{A}(s), \tag{10}$$

where $\tilde{\mathbf{u}}^E(s)$ and $\tilde{\mathbf{u}}_i^A(s)$ $(i = 1,\ldots,n)$ represent the nodal DoFs vectors associated with the elastic and anelastic strains, respectively. To take into consideration this relaxation the entire anelastic displacement field itself may be comprised of several individual fields where n series of anelastic DoFs are considered. Furthermore, the anelastic (dissipative) variables series might be related with the elastic variables by

$$\tilde{\mathbf{u}}_i^A(s) = \frac{\Omega_i}{s+\Omega_i}\tilde{\mathbf{u}}(s), \tag{11}$$

and the elastic displacements that appear in strain energy expressions are replaced by the difference between the total and anelastic displacements,

$$\tilde{\mathbf{u}}^E(s) = \tilde{\mathbf{u}}(s) - \sum_{i=1}^{n}\tilde{\mathbf{u}}_i^A(s) = \sum_{i=1}^{n}\frac{s}{s+\Omega_i}\tilde{\mathbf{u}}(s). \tag{12}$$

Neglecting the initial conditions and substituting Equation (8) into (9) yields

$$\Big[s^2\mathbf{M}_{uu} + s\mathbf{D}_{uu} + \mathbf{K}_{uu}^{EP*} + G_0\bar{\mathbf{K}}_{uu}^{V}\Big(1 + \sum_{i=1}^{n}\frac{\Delta_i s}{s+\Omega_i}\Big)\Big]\tilde{\mathbf{u}}(s) = \tilde{\mathbf{F}}(s). \tag{13}$$

Then, substituting Equation (12) into (13) yields

$$\Big(s^2\mathbf{M}_{uu} + s\mathbf{D}_{uu} + \mathbf{K}_{uu}^{EP*} + \mathbf{K}_{uu}^{V0}\Big)\tilde{\mathbf{u}}(s) + \mathbf{K}_{uu}^{V0}\sum_{i=1}^{n}\Delta_i\Big(\tilde{\mathbf{u}}(s) - \tilde{\mathbf{u}}_i^A(s)\Big) = \tilde{\mathbf{F}}(s), \tag{14}$$

where $\mathbf{K}_{uu}^{V0} = G_0\bar{\mathbf{K}}_{uu}^{V}$. Considering Equations (11) and (14), after some algebra we get the following coupled system,

$$\Big(s^2\mathbf{M}_{uu} + s\mathbf{D}_{uu} + \mathbf{K}_{uu}^{EP*} + \mathbf{K}_{uu}^{V\infty}\Big)\tilde{\mathbf{u}}(s) - \mathbf{K}_{uu}^{V0}\sum_{i=1}^{n}\Delta_i\tilde{\mathbf{u}}_i^A(s) = \tilde{\mathbf{F}}(s), \tag{15a}$$

$$\Big(\frac{s}{\Omega_i} + 1\Big)\tilde{\mathbf{u}}_i^A(s) - \tilde{\mathbf{u}}(s) = \mathbf{0}, \tag{15b}$$

where

$$\mathbf{K}_{uu}^{V\infty} = \Big(1 + \sum_{i=1}^{n}\Delta_i\Big)\mathbf{K}_{uu}^{V0}.$$

In order to overcome some of the shortcomings of frequency models, the frequency- or time-dependent behavior of the viscoelastic material should be captured by using a time-domain model. Thus, multiplying Equation (15b) by $\Delta_i\mathbf{K}_{uu}^{V0}$ and since all matrices are independent of s, the time domain system is obtained by the inverse Laplace transform of Equations (15), yielding

$$\mathbf{M}_{uu}\ddot{\bar{\mathbf{u}}}(t) + \mathbf{D}_{uu}\dot{\bar{\mathbf{u}}}(t) + \Big(\mathbf{K}_{uu}^{EP*} + \mathbf{K}_{uu}^{V\infty}\Big)\bar{\mathbf{u}}(t) - \mathbf{K}_{uu}^{V0}\sum_{i=1}^{n}\Delta_i\bar{\mathbf{u}}_i^A(t) = \mathbf{F}(t), \tag{16a}$$

$$\frac{\Delta_i}{\Omega_i}\mathbf{K}_{uu}^{V0}\dot{\bar{\mathbf{u}}}_i^A(t) + \Delta_i\mathbf{K}_{uu}^{V0}\bar{\mathbf{u}}_i^A(t) - \Delta_i\mathbf{K}_{uu}^{V0}\bar{\mathbf{u}}(t) = \mathbf{0}. \tag{16b}$$

Equations (16) define a coupled system which may be expressed as

$$\bar{\mathbf{M}}\ddot{\bar{\mathbf{q}}}(t) + \bar{\mathbf{D}}\dot{\bar{\mathbf{q}}}(t) + \bar{\mathbf{K}}\bar{\mathbf{q}}(t) = \bar{\mathbf{F}}(t), \tag{17}$$

where

$$\bar{\mathbf{M}} = \begin{bmatrix} \mathbf{M}_{uu} & \mathbf{0} \\ \mathbf{0} & \mathbf{0} \end{bmatrix}, \ \bar{\mathbf{D}} = \begin{bmatrix} \mathbf{D}_{uu} & \mathbf{0} \\ \mathbf{0} & \mathbf{D}_{AA} \end{bmatrix}, \ \bar{\mathbf{K}} = \begin{bmatrix} \mathbf{K}_{EE} & \mathbf{K}_{EA} \\ \mathbf{K}_{AE} & \mathbf{K}_{AA} \end{bmatrix},$$

$$\bar{\mathbf{q}}(t) = \text{col}\Big(\bar{\mathbf{u}}(t), \bar{\mathbf{u}}_1^A(t), \ldots, \bar{\mathbf{u}}_n^A(t)\Big), \ \bar{\mathbf{F}}(t) = \text{col}\Big(\mathbf{F}(t), \mathbf{0}, \ldots, \mathbf{0}\Big),$$

and

$$\mathbf{D}_{AA} = \text{diag}\Big(\frac{\Delta_1}{\Omega_1}\mathbf{K}_{uu}^{V0}, \ldots, \frac{\Delta_n}{\Omega_n}\mathbf{K}_{uu}^{V0}\Big), \ \mathbf{K}_{AA} = \text{diag}\Big(\Delta_1\mathbf{K}_{uu}^{V0}, \ldots, \Delta_n\mathbf{K}_{uu}^{V0}\Big),$$

$$\mathbf{K}_{EE} = \mathbf{K}_{uu}^{EP*} + \mathbf{K}_{uu}^{V\infty}, \ \mathbf{K}_{EA} = \left[-\Delta_1\mathbf{K}_{uu}^{V0}, \ldots, -\Delta_n\mathbf{K}_{uu}^{V0}\right], \ \mathbf{K}_{AE} = \mathbf{K}_{EA}^{\mathrm{T}}.$$

In Equation (17) the number of anelastic DoFs of the system, for each ADF series, must be equal to the number of elastic DoFs. However, model reduction techniques might be utilized in order to reduce the size of the system. As suggested in [29] the matrices corresponding to the dissipative (anelastic) DoFs might be reduced and diagonalized to reduce the computational cost. Considering a modal projection such that $\bar{\mathbf{u}}_i^A(t) = \boldsymbol{\Psi}_A\hat{\mathbf{u}}_i^A(t)$ and $\boldsymbol{\Lambda}_A = \boldsymbol{\Psi}_A^{\mathrm{T}}\mathbf{K}_{uu}^{V0}\boldsymbol{\Psi}_A$ is a diagonal matrix composed by the non zero eigenvalues of $\mathbf{K}_{uu}^{V0}$ and $\boldsymbol{\Psi}_A$ the correspondent matrix of normalized eigenvectors such that $\boldsymbol{\Psi}_A^{\mathrm{T}}\boldsymbol{\Psi}_A = \mathbf{I}$, the order of the system can be reduced and matrices $\mathbf{D}_{AA}$, $\mathbf{K}_{AA}$ and $\mathbf{K}_{AE}$ become

$$\mathbf{D}_{AA} = \text{diag}\Big(\frac{\Delta_1}{\Omega_1}\boldsymbol{\Lambda}_A, \ldots, \frac{\Delta_n}{\Omega_n}\boldsymbol{\Lambda}_A\Big), \ \mathbf{K}_{AA} = \text{diag}\Big(\Delta_1\boldsymbol{\Lambda}_A, \ldots, \Delta_n\boldsymbol{\Lambda}_A\Big),$$

$$\mathbf{K}_{EA} = \left[-\Delta_1\mathbf{K}_{uu}^{V0}\boldsymbol{\Psi}_A, \ldots, -\Delta_n\mathbf{K}_{uu}^{V0}\boldsymbol{\Psi}_A\right],$$

where the vector of DoFs is modified to $\hat{\mathbf{q}}(t) = \text{col}\Big(\bar{\mathbf{u}}(t), \hat{\mathbf{u}}_1^A(t), \ldots, \hat{\mathbf{u}}_n^A(t)\Big)$. In the case where only some part of the beam is covered with viscoelastic layers only some FEs have viscoelastic components and $\mathbf{K}_{uu}^{V0}$ can have several rows and columns of zeros which in turn leads to some zero eigenvalues. Thus, the size of $\hat{\mathbf{u}}_i^A(t)$ can be substantially smaller than that of $\bar{\mathbf{u}}_i^A(t)$. Furthermore, one may notice from $\bar{\mathbf{M}}$ that the anelastic DoFs have no inertia and therefore the global mass matrix $\bar{\mathbf{M}}$ is singular and is not positive-definite. However, the singularity of the mass matrix can be overcome if instead of solving the second-order system (17) one considers a state-space representation with an adequate design of the state variables. Moreover, the number of flexible modes is kept the same and the dissipative modes, which correspond to the internal relaxations of the viscoelastic material, are overdamped with a lower observability.

2.3 State Space Design

The state space approach is the basis of the modern control theories and is strongly recommended in the design and analysis of control systems with a great amount of inputs and outputs. In this method, dynamic systems are described by a set of first-order differential equations in variables called the *state*. See related textbooks in references [30, 31].

To apply the augmented FE model due to the ADF modelling of the viscoelastic layers in control design, the system in Equation (17) is transformed into a state space form. Therefore, in order to overcome the singularity of the mass matrix the state space vector $\mathbf{x}(t)$ is chosen as

$$\mathbf{x}(t)=\left\{ \begin{array}{c} \hat{\mathbf{q}}(t) \\ \dot{\hat{\mathbf{u}}}(t) \end{array} \right\}, \tag{18}$$

where the state variables are the modal projected augmented vector $\hat{\mathbf{q}}(t)$ and the the time derivative of the mechanical DoFs vector $\dot{\hat{\mathbf{u}}}(t)$. It's worthy to note that the time derivatives of the anelastic DoFs vectors $\hat{\mathbf{u}}_i^A(t)$ are not considered here since these variables are massless. Thus, the coupled system in Equation (17) and the sensing Equation (6b) can be expressed in terms of the state variables vector $\mathbf{x}(t)$, yielding

$$\dot{\mathbf{x}}(t) = \mathbf{A}\mathbf{x}(t) + \mathbf{B}_\phi \mathbf{u}_\phi(t) + \mathbf{B}_u \mathbf{u}_u(t), \tag{19a}$$

$$\mathbf{y}(t) = \mathbf{C}\mathbf{x}(t), \tag{19b}$$

where $\mathbf{A}$ is the system matrix, $\mathbf{B}_u$ and $\mathbf{B}_\phi$ are the mechanical and electrical input matrices associated with the mechanical and electrical loads, $\mathbf{C}$ is the output matrix, $\mathbf{u}_u(t)$ and $\mathbf{u}_\phi(t)$ are the mechanical and electrical input vectors and $\mathbf{y}(t)$ is the output vector, given by

$$\mathbf{A} = \left[\begin{array}{ccc} \mathbf{0} & \mathbf{0} & \mathbf{I} \\ -\mathbf{D}_{AA}^{-1}\mathbf{K}_{AE} & -\mathbf{D}_{AA}^{-1}\mathbf{K}_{AA} & \mathbf{0} \\ -\mathbf{M}_{uu}^{-1}\mathbf{K}_{EE} & -\mathbf{M}_{uu}^{-1}\mathbf{K}_{EA} & -\mathbf{M}_{uu}^{-1}\mathbf{D}_{uu} \end{array} \right],$$

$$\mathbf{B}_u = \left[\begin{array}{c} \mathbf{0} \\ \mathbf{0} \\ \mathbf{M}_{uu}^{-1} \end{array} \right], \ \mathbf{B}_\phi = \left[\begin{array}{c} \mathbf{0} \\ \mathbf{0} \\ -\mathbf{M}_{uu}^{-1}\mathbf{K}_{u\phi\mathrm{a}} \end{array} \right],$$

$$\mathbf{C} = \left[\begin{array}{ccc} -\mathbf{K}_{\phi\phi\mathrm{s}}^{-1}\mathbf{K}_{\phi u\mathrm{s}} & \mathbf{0} & \mathbf{0} \\ \mathbf{0} & \mathbf{0} & -\mathbf{K}_{\phi\phi\mathrm{s}}^{-1}\mathbf{K}_{\phi u\mathrm{s}} \\ \mathbf{I} & \mathbf{0} & \mathbf{0} \\ \mathbf{0} & \mathbf{0} & \mathbf{I} \end{array} \right], \ \mathbf{y}(t) = \left\{ \begin{array}{c} \bar{\boldsymbol{\phi}}_\mathrm{s}(t) \\ \dot{\bar{\boldsymbol{\phi}}}_\mathrm{s}(t) \\ \mathbf{u}(t) \\ \dot{\mathbf{u}}(t) \end{array} \right\},$$

$$\mathbf{u}_u(t) = \mathbf{F}_u(t), \ \mathbf{u}_\phi(t) = \bar{\boldsymbol{\phi}}_\mathrm{a}(t),$$

As presented by Vasques and Rodrigues [18], the signal induced by the piezoelectric sensors should be calculated from an average of the electrical DoFs where an electrical FE separation of the electrodes was performed. Furthermore, the modal projected definitions of matrices $\mathbf{D}_{AA}$, $\mathbf{K}_{AA}$ and $\mathbf{K}_{EA}$ should be used in order to reduce the size of the system leading to a lower computational cost.

2.4 Modal Reduction of the State Space Model

In the process of designing an active control system one can utilize a full model of the system and, consequently, a higher computational effort is needed, or a reduced model of the system, which requires a lower computational effort. However, the structural mathematical model and

controller design are not independent aspects of vibration control. Flexible structures are distributed parameter systems that have an infinite number of DoF, and a feedback controller based on a reduced modal model can destabilize the residual modes (unmodeled dynamics) leading to observation and control spillover problems. They both degrade the system's performance, and the former can even cause the system to become unstable [5]. Methods to reduce the effects of spillover are discussed by Balas [32].

One major disadvantage in using internal variables models such as the ADF to model the damping introduced by the viscoelastic materials is the creation of additional dissipation coordinates. Even with a modal reduction of the DoFs of the non viscoelastic elements the order of the system quickly increases as the number of series of dissipation ADF parameters used in the summation is increased. This size is determined by the number of series of parameters necessary for an accurate curve fitting of the frequency-dependent complex shear modulus. Larger order makes control design more difficult, especially when these states are non-physical and can not be directly sensed [33]. It is therefore advantageous to look at model reduction to reduce the system's size.

There are many methods on model reduction in structural dynamics. The aims are to approximate the original state space system by an equivalent system with a lower dimension. That can be achieved by a complex modal projection of the original system and a subsequent truncation of the number of modes considered. Thus, the complex eigensolution of the system matrix $\mathbf{A}$ is derived such that

$$\mathbf{A}\boldsymbol{\Psi}_R = \boldsymbol{\Lambda}\boldsymbol{\Psi}_R,\ \mathbf{A}^{\mathrm{T}}\boldsymbol{\Psi}_L = \boldsymbol{\Lambda}\boldsymbol{\Psi}_L, \tag{20}$$

where $\boldsymbol{\Psi}_R$ and $\boldsymbol{\Psi}_L$ are the right and left complex eigenvectors matrices normalized by $\boldsymbol{\Psi}_L^{\mathrm{T}}\boldsymbol{\Psi}_R = \mathbf{I}$ and $\boldsymbol{\Lambda}$ the correspondent eigenvalues matrix. However, if one looks at the complex eigenvalues of $\mathbf{A}$ one finds that some of them are underdamped, usually associated with the elastic DoFs, and other overdamped ones, which are associated with the dissipative DoFs. Thus, considering a modal decomposition of the eigensolution in the underdamped and overdamped modes yields

$$\boldsymbol{\Lambda} = \begin{bmatrix} \boldsymbol{\Lambda}_U & \mathbf{0} \\ \mathbf{0} & \boldsymbol{\Lambda}_O \end{bmatrix},\ \boldsymbol{\Psi}_R = \begin{bmatrix} \boldsymbol{\Psi}_{RU} & \boldsymbol{\Psi}_{RO} \end{bmatrix},\ \boldsymbol{\Psi}_L = \begin{bmatrix} \boldsymbol{\Psi}_{LU} & \boldsymbol{\Psi}_{LO} \end{bmatrix}, \tag{21}$$

where the subscripts $(\cdot)_U$ and $(\cdot)_O$ are used to denote the underdamped and overdamped counterparts of the complex eigensolution. Since the contribution of the overdamped modes to the dynamic response of the system is negligible the state space vector can be approximated only by the contribution of the elastic (underdamped) modes such that $\mathbf{x}(t) \approx \boldsymbol{\Psi}_{RU}\mathbf{x}_U(t)$ and the state space system in Equations (19) is reduced to a state space modal system with the same outputs and state space vector $\mathbf{x}_U(t)$, given by

$$\dot{\mathbf{x}}_U(t) = \boldsymbol{\Lambda}_U\mathbf{x}_U(t) + \boldsymbol{\Psi}_{LU}^{\mathrm{T}}\mathbf{B}_\phi\mathbf{u}_\phi(t) + \boldsymbol{\Psi}_{LU}^{\mathrm{T}}\mathbf{B}_u\mathbf{u}_u(t), \tag{22a}$$

$$\mathbf{y}(t) = \mathbf{C}\boldsymbol{\Psi}_{RU}\mathbf{x}_U(t). \tag{22b}$$

However, when excited a structure presents preferable modes of vibration which depend of the spectral content of the excitation. Assuming that the lower order modes, which have lower energy associated and consequently are the more easily excitable ones, are the more significant

to the global response of the system in the frequency range of interest, a truncated complex modal matrix $\hat{\mathbf{\Psi}}_{RU}$ can be utilized instead where only the first r modes are considered,

$$\mathbf{x}(t) \approx \sum_{i=1}^{r} \mathbf{\Psi}_{RU}^{i} x_U^i(t) = \hat{\mathbf{\Psi}}_{RU} \hat{\mathbf{x}}_U(t), \tag{23}$$

where $\hat{\mathbf{\Psi}}_{RU} = [\mathbf{\Psi}_{RU}^1, \cdots, \mathbf{\Psi}_{RU}^r]$ is the truncated modal matrix and $\hat{\mathbf{x}}_U(t) = \{x_U^1(t), \cdots, x_U^r(t)\}^{\mathrm{T}}$ the correspondent modal coordinates vector. Hence, the system's size isn't anymore the total number of DoFs of the FE model but twice the number of modes chosen to model it. Finally, considering the correspondent underdamped eigenvalues truncated matrix $\hat{\mathbf{\Lambda}}_U$, the state space system in Equations (19) is reduced to a truncated state space modal system with the same outputs and truncated state space vector $\hat{\mathbf{x}}_U(t)$, given by

$$\dot{\hat{\mathbf{x}}}_U(t) = \hat{\mathbf{\Lambda}}_U \hat{\mathbf{x}}_U(t) + \hat{\mathbf{\Psi}}_{LU}^{\mathrm{T}} \mathbf{B}_\phi \mathbf{u}_\phi(t) + \hat{\mathbf{\Psi}}_{LU}^{\mathrm{T}} \mathbf{B}_u \mathbf{u}_u(t), \tag{24a}$$

$$\mathbf{y}(t) = \mathbf{C} \hat{\mathbf{\Psi}}_{RU} \hat{\mathbf{x}}_U(t). \tag{24b}$$

3 CONTROL SYSTEM ARCHITECTURE DESIGN

3.1 Feedback Control

The ultimate aim of the feedback control is often to reduce the motion of the mechanical system to the greatest possible extent and, in that case, the control system is said to act as a *regulator*. Systems where direct methods of designing feedback control systems which achieve the greatest possible reduction in the dynamic response are used, are known as *optimal control* systems and classical textbooks about the subject can be found in references [30, 31].

For the sake of clarity the development of the following equations is done taking into consideration the conventional notation tipically utilized by the control comunity to denote a state space system, as represented in Equations (19). However, for the present state space model of beams with ACLD treatments, the reduced system in Equations (24) should be used instead, and the respective correspondence between vectors and matrices between Equations (19) and (24) should be made.

In optimal control theory the feedback control system is designed to minimize a cost function, or performance index, which is proportional to the required measure of the system's response and to the control inputs required to attenuate the response. When the control system is designed to operate for a long period of time the cost function can be reasonably chosen to be quadratically dependent on the system states and control input, given by

$$J = \int_0^\infty \left[\mathbf{x}^{\mathrm{T}}(t) \mathbf{Q}_x \mathbf{x}(t) + \mathbf{u}_\phi^{\mathrm{T}}(t) \mathbf{R} \mathbf{u}_\phi(t) \right] \mathrm{d}t, \tag{25}$$

where $\mathbf{Q}_x$ and $\mathbf{R}$ are the state variable and control input weighting matrices.

The present work considers an approach to control system design where the dynamics of the mechanical system is considered in terms of its modal response. Since the truncated state space modal system presented in Equations (24) is composed of underdamped complex conjugated modes the obtained state space matrices terms are presented in complex conjugated pairs. This

may constitute a problem for controller design. Thus, as suggested by Meirovitch [5] or Friot [34], the system can be represented by an equivalent system with real matrices where in this case the new (transformed) states are not the modal amplitudes but something related with them, while the outputs of the system remain the same. Hence, one may choose as a performance index the cost function minimizing the new state variables (related with the modal amplitudes).

By a convenient definition of the state weighting matrix $\mathbf{Q}_x$, the modal gain matrix can be 'tuned' to give different design objectives. Assuming that all the modes (state variables) are observable and controllable, the cost function in Equation (25) provides independent control over the natural frequencies and damping ratios of each mode. That strategy is called *Independent Modal-Space Control* (IMSC) [5]. Some convenient choices for the definition of the weighting matrices can be, for example, $\mathbf{R}$ =diag$(\mathbf{I}, \mathbf{I})$ and $\mathbf{Q}_x$ =diag$(\mathbf{\Omega}, \mathbf{0})$, where $\mathbf{I}$ is the identity matrix and $\mathbf{\Omega}$ a diagonal matrix, with the generic term ω_i^2 (squared natural frequency of the ith mode), of size $(r \times r)$, with r being the number of modes of the truncated modal model.

It can be seen in references [30, 31] that the feedback control system which minimizes the cost function in Equation (25), for the linear time-invariant equivalent real system of Equations (24), uses state feedback with a sub-optimal feedback gain matrix $\mathbf{K}_g$, so that

$$\mathbf{u}_\phi(t) = -\mathbf{K}_g \mathbf{x}(t). \tag{26}$$

Since the feedback gains typically approach steady-state values far from the initial time, a steady-state controller is utilized with a steady-state feedback gain matrix given by $\mathbf{K}_g = \mathbf{R}^{-1}\mathbf{B}_\phi^{\mathrm{T}}\mathbf{P}$, where $\mathbf{P}$ is the steady state solution of the *matrix Riccati equation*,

$$\mathbf{P}\mathbf{A} + \mathbf{A}^{\mathrm{T}}\mathbf{P} + \mathbf{Q}_x - \mathbf{P}\mathbf{B}_\phi\mathbf{R}^{-1}\mathbf{B}_\phi^{\mathrm{T}}\mathbf{P} = \mathbf{0}. \tag{27}$$

This control philosophy is called the steady-state *Linear Quadratic Regulator* (LQR).

Thus, considering the feedback law in Equation (26), the closed-loop state equation is given by

$$\dot{\mathbf{x}}(t) = (\mathbf{A} - \mathbf{B}_\phi\mathbf{K}_g)\,\mathbf{x}(t) + \mathbf{B}_u\mathbf{u}_u(t). \tag{28}$$

In the previous equation it was assumed that all the states were completely observable and therefore could be directly related to the outputs and used by the control system. However, that is not always the case and a more realistic approach would consider that only some of the outputs $\mathbf{y}(t)$ can be known and measured. In order to be able to use the states information in the control system, it will be necessary to estimate the states from a model of the system and a limited number of observations of the outputs. That estimation is made usually by a *state estimator* or *observer*.

The state variable estimates are very sensitive to any uncorrelated noise in the system, particularly measurement noise from the observed outputs of the mechanical system. Knowing the statistical properties of the various sources of noise in the mechanical system, and assuming white uncorrelated noise uniformly distributed in the bandwidth, an 'optimal' state observer which minimizes the effects of plant and measurement noise is known as *Kalman-Bucy filter*. In a similar way to the steady-state LQR, the 'optimal' Kalman-Bucy gain matrix typically experiences a transient and then approaches steady-state as time increases from the initial time. In

applications where the estimator is designed to operate for time periods that are long compared to the transient times of the Kalman-Bucy gains, it is reasonable to ignore the transient and exclusively use the steady-state gains $\mathbf{K}_e$. The equations for computing the Kalman-Bucy gain have a striking resemblance to the equations for computing the LQR gain. As pointed out by Burl [30] the steady-state Kalman-Bucy filter problem is shown to be mathematically equivalent to the steady-state LQR problem when appropriate substitutions are made.

Combining the steady-state Kalman-Bucy filter with the steady state LQR, the inter-related dynamic system will take the form

$$\begin{Bmatrix} \dot{\mathbf{x}}(t) \\ \dot{\mathbf{e}}(t) \end{Bmatrix} = \begin{bmatrix} \mathbf{A} - \mathbf{B}_\phi \mathbf{K}_g & \mathbf{B}_\phi \mathbf{K}_g \\ \mathbf{0} & \mathbf{A} - \mathbf{K}_e \mathbf{C} \end{bmatrix} \begin{Bmatrix} \mathbf{x}(t) \\ \mathbf{e}(t) \end{Bmatrix} + \begin{bmatrix} \mathbf{B}_u \\ \mathbf{B}_u \end{bmatrix} \mathbf{u}_u(t) + \begin{bmatrix} \mathbf{B}_w & \mathbf{0} \\ \mathbf{B}_w & -\mathbf{K}_e \end{bmatrix} \begin{Bmatrix} \mathbf{w}(t) \\ \mathbf{v}(t) \end{Bmatrix}, \tag{29}$$

where $\dot{\mathbf{e}}(t)$ is the error between the true and estimated states, $\mathbf{B}_w$ is the plant noise input matrix, and $\mathbf{w}(t)$ and $\mathbf{v}(t)$ are the plant and measurement noise vectors. The plant and measurement noise are both assumed to be white, have a gaussian probability density function and are assumed uncorrelated with the inputs. The correlation properties of the plant and measurement noise vectors are given by the correlation matrices

$$E\left[\mathbf{B}_w \mathbf{w}(t) \mathbf{w}^{\mathrm{T}}(t) \mathbf{B}_w^{\mathrm{T}}\right] = \mathbf{W}, \quad E\left[\mathbf{v}(t) \mathbf{v}^{\mathrm{T}}(t)\right] = \mathbf{V}, \tag{30}$$

where E denotes the expectation operator.

Because we must assume that the random perturbations (force disturbance or measurement noise) are gaussian, this control philosophy is called *Linear Quadratic Gaussian* (LQG) control. The dynamics of the coupled controller and observer system is determined by the eigenvalues of the system matrix in Equation (29) and the closed-loop coupled system stability depends of the two sub-systems. The error will asymptotically be stable provided the observer poles have negative real components collocated, in the complex plan, as far as possible from the system poles so that the observer error reduces more rapidly than the system response. A comprehensive study concerning feedback control theories can be found in reference [35].

3.2 Feedforward Control

Feedforward control system design and implementation rely upon digital filtering fundamentals and adaptive filter theory, which can be found in reference textbooks such as [9, 36, 37]. Contrarily to feedback systems, feedforward control assumes that one has information about the original (primary) excitation of the system and that a reference signal correlated with the excitation is available. The aims are then to produce a secondary excitation that will cancel the effects of the primary excitation at the chosen location.

The *filtered-reference LMS* algorithm is the most widely accepted feedforward control algorithm because of its ease of implementation and remarkable performance. In Figure 2 a schematic diagram of the discrete-time (digital) generalized plant for a hybrid, combined feedback/feedforward, controller is presented. It is assumed that a detection system, which produces

a signal correlated with the primary disturbance, exists (or not, and in that case the true excitation signal is utilized), and produces a reference signal $r(k)$ correlated with the excitation. This signal is then adaptively filtered to generate the necessary control action, u_ϕ^{ff}, to cancel the effect of the primary excitation (disturbance).

The control filtering process utilizes an adaptive finite impulse response (FIR) filter whose ith coefficient at the kth sample time is $h_i(k)$. The filter output $u_\phi^{ff}(k)$ is obtained from

$$u_\phi^{ff}(k) = \sum_{i=0}^{N} h_i(k) r(k-i), \tag{31}$$

where $N+1$ is the number of filter coefficients. Then, the control signal has to pass through a part of the physical system before the error sensor measures the output. This physical path, $P_\phi(z)$, is called the *cancelation path* (or error path). Therefore, the output of the plant due to the feedforward control input only is given by

$$y_\phi(k) = \sum_{j=0}^{M} g_j \sum_{i=0}^{N} h_i(k) r(k-i-j), \tag{32}$$

where g_j is the discrete impulse response of the control input-to-output path $P_\phi(z)$, which is assumed to be of order L. Thus, the net output of the system, $y(k)$, can be written as

$$y(k) = y_u(k) + \sum_{j=0}^{M} g_j \sum_{i=0}^{N} h_i(k) r(k-i-j). \tag{33}$$

However, the order of convolution can be interchanged without changing the result, yielding

$$y(k) = y_u(k) + \sum_{i=0}^{N} h_i(k) \bar{r}(k-i), \tag{34}$$

where

$$\bar{r}(k-i) = \sum_{j=0}^{M} g_j r(k-i-j). \tag{35}$$

By rearranging the convolution, a signal $\bar{r}(k-i)$ is created, which is to be estimated by the filtered-reference operation. If the true impulse response of the plant $P_\phi(z)$ is estimated by an FIR or infinite impulse response (IIR) filter, then an estimate of $\bar{r}(k)$ is given as $\hat{r}(k)$.

The problem of how best to adapt the filter coefficients $h_i(k)$ can now be addressed. They can be adapted in order to minimize a cost function quadratically dependent of the output, $J = E[y^2(k)]$. However, as for the LMS algorithm [36], the instantaneous value of $y^2(k)$ is used as an estimate of the expected value of J. A simple gradient descent algorithm is thus guaranteed to converge to the globally optimal solution of the problem of minimizing the cost function. Such an adaptive algorithm can be written as

$$h_i(k+1) = h_i(k) - \mu \frac{\partial J}{\partial h_i(k)}, \tag{36}$$

where μ is a convergence coefficient. Thus, from the definition of the cost function the derivative

in Equation (36) is written as

$$\frac{\partial J}{\partial h_i(k)} = 2y(k)\frac{\partial y(k)}{\partial h_i(k)}. \tag{37}$$

From Equation (34) the derivative of $y(k)$ with respect to $h_i(k)$ is simply $\bar{r}(k-i)$. If one uses the estimated filtered reference signal $\hat{r}(k-i)$, the steepest descent algorithm required to adapt the coefficients of the digital controller, given by Equation (36), can thus be written as

$$h_i(k+1) = h_i(k) - \alpha y(k)\hat{r}(k-i), \tag{38}$$

where $\alpha = 2\mu$ is another convergence coefficient parameter that determines the speed and stability of adaptation. The convergence properties of the filtered-reference LMS algorithm are similar to those of the normal LMS algorithm, whose properties are described in detail by Widrow and Stearns [36], for example.

3.3 Combined Feedback/Feedforward Control

Combined feedback/feedforward (hybrid) control is defined as the combination of both feedback and adaptive feedforward control, as outlined in [7], and a schematic diagram of the discrete-time (digital) generalized plant for a SISO control system is depicted in Figure 2. The primary purpose of hybrid control systems is to design the disturbance control problem with the architecture best suited for overall performance. If a reverberant plant is exposed to exogenous inputs consisting of both stochastic and harmonic disturbances, for which a reference correlated with the harmonic disturbance is available, it is likely that feedback control strategies are best suited for the stochastic disturbances, while adaptive feedforward control strategies are better suited for the harmonic disturbances. Hybrid control utilizes both forms of control to maximize the performance of the adaptive structure to mixed-signal disturbances. The essential features of hybrid control for adaptive structures are: robust disturbance rejection of narrowband, periodic signals; simultaneous transient suppression of impulsive and stochastic disturbances; improved performance and convergence of the adaptive, feedforward controller.

4 CASE STUDY

The primary purpose of this case study is to investigate the design of feedback, adaptive feedforward and combined feedback/feedforward (hybrid) vibration suppression of a beam with a partial symmetrically collocated ACLD treatment (viscoelastic layers sandwiched between the piezoelectric patches and the base beam). With this purpose, the FE and ADF model previously presented were implemented in Matlab® and the control algorithms were simulated with Simulink®. The structural response is assumed to derive from the presence of either periodic or stochastic point-force disturbances. First, an optimal LQG controller is designed to mitigate the effects of stochastic disturbances. Then, an adaptive feedforward controller (filtered-reference LMS) is implemented for a periodic disturbance, and the final example combines both the feedback and adaptive feedforward elements to realize a hybrid controller.

The cantilever aluminium beam with the ACLD patches is depicted in Figure 3. The beam

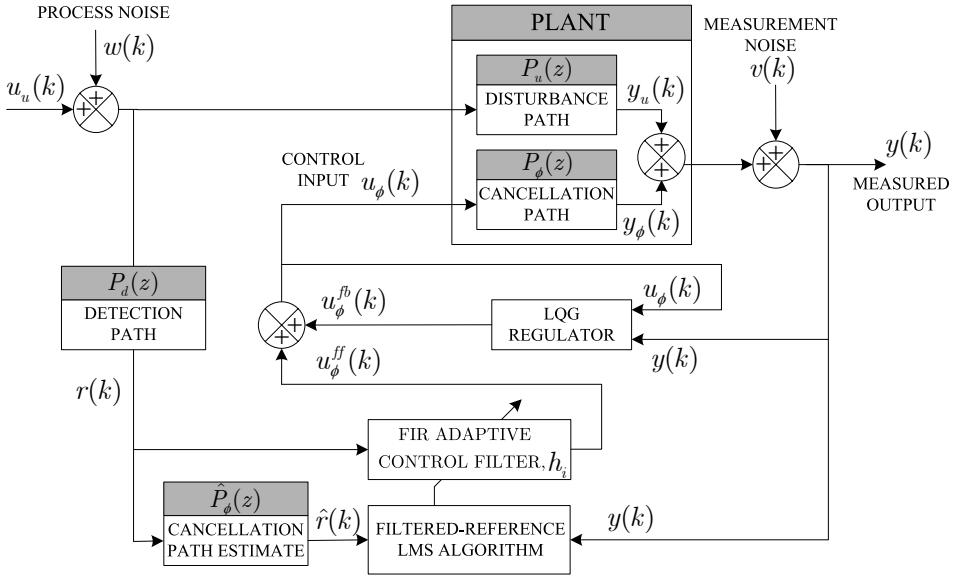

Figure 2. Schematic diagram of the discrete-time generalized plant for the combined feedback/feedforward (hybrid) SISO controller.

is $300\,\mathrm{mm}$ long and $2\,\mathrm{mm}$ thick, the partial ACLD treatment is $70\,\mathrm{mm}$ long, with viscoelastic and piezoelectric layers of thickness $0.03\,\mathrm{mm}$ and $1\,\mathrm{mm}$, respectively, and the symmetrically collocated ACLD treatment is positioned $4\,\mathrm{mm}$ away from the clamped edge. The mechanical and electrical material properties of the passive viscoelastic layers, 3M ISD112 [38], and of the piezoelectric constraining patches, PXE-5, are presented in Table 1 (see the IEEE standard [16] for details about notation). The shear storage modulus and loss factor of the viscoelastic material at the $27\,^{\circ}\mathrm{C}$, presented in Figure 4, were defined by means of a three-series ADF model with parameters $G_0 = 0.5\,\mathrm{MPa}$, $\Delta = [0.743, 3.265, 43.284]$, $\Omega = [468.7, 4742.4, 71532.5]\,\mathrm{rad/\,s}$, which were determined by curve fitting experimental data in the frequency range $20 - 5000\,\mathrm{Hz}$ [29]. Furthermore, the Young's storage modulus was obtained assuming a frequency independent Poisson's ratio equal to 0.45.

Aluminium		3M ISD 112		PXE-5			
E	$70\,\mathrm{GPa}$	G	Figure 4	c_{11}^E	$131.1\,\mathrm{GPa}$	d_{31}	$-215\times10^{-12}\,\mathrm{m\,V^{-1}}$
ν	0.3	ν	0.45	c_{12}^E	$7.984\,\mathrm{GPa}$	d_{33}	$500\times10^{-12}\,\mathrm{m\,V^{-1}}$
ρ	$2710\,\mathrm{kg\,m^{-3}}$	ρ	$1600\,\mathrm{kg\,m^{-3}}$	c_{13}^E	$8.439\,\mathrm{GPa}$	d_{15}	$515\times10^{-12}\,\mathrm{m\,V^{-1}}$
				c_{33}^E	$12.31\,\mathrm{GPa}$	$\varepsilon_{11}^T/\varepsilon_0$	1800
				c_{44}^E	$2.564\,\mathrm{GPa}$	$\varepsilon_{33}^T/\varepsilon_0$	2100
				c_{66}^E	$2.564\,\mathrm{GPa}$	ρ	$7800\,\mathrm{kg\,m^{-3}}$

Table 1. Material properties of the aluminium, PXE-5 and 3M ISD112.

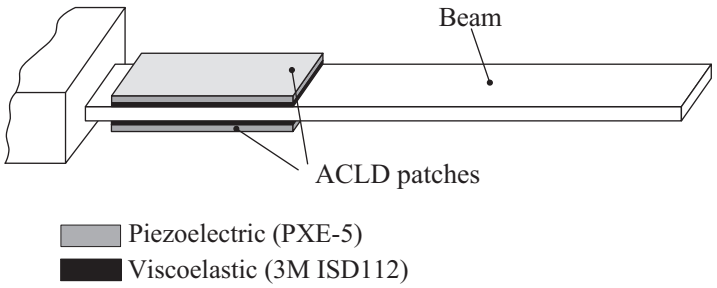

Figure 3. Clamped beam with a pair of ACLD patches.

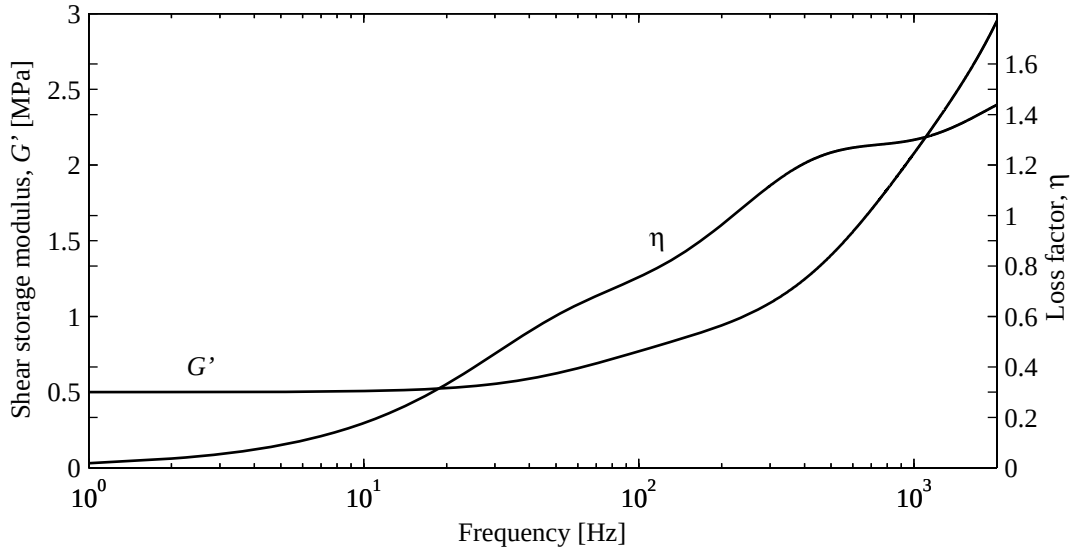

Figure 4. Frequency dependent properties of 3M ISD112 at $27\,^{\circ}\mathrm{C}$ defined through a three-series ADF model.

In order to infer the amount of damping introduced by the PCLD treatment, the length of the piezoelectric constraining layer was defined according to the maximum length of commercially available piezoelectric actuators. Then, a geometric optimization study, through a parametric study of the influence of only varying the thickness of the viscoelastic layers in the overall damping performance of the PCLD treatment, was performed. The beam was discretized into 150 equal length FEs, with a layerwise (discrete-layer) configuration of 1/1/3/1/1 for the five physical layers, a state space model with 20 modes with a modal damping ratio equal to 0.2% for all the modes was considered, and the operating temperature was supposed to be constant and equal to $27\,^{\circ}\mathrm{C}$. The damping ratios of the first five modes for viscoelastic thickness in the range $0.001 - 1\,\mathrm{mm}$ are presented in Figure 5.

From the analysis of Figure 5, one can see that the optimal thickness depends on the frequency range (modes) to attenuate, with the maximum values of damping ratio occurring at

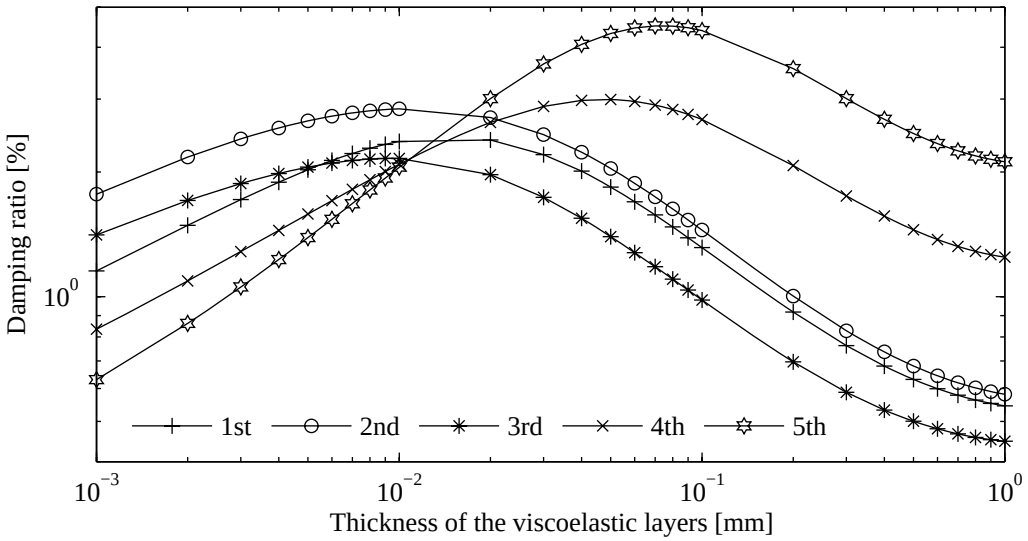

Figure 5. Influence of the viscoelastic layers thickness on the modal damping ratios of the beam with PCLD treatment.

different thickness. Furthermore, it can be seen that the optimal thickness for the first three modes is comprised in the range $0.01 - 0.02\,\mathrm{mm}$, and for the higher frequency modes in the range $0.05 - 0.08\,\mathrm{mm}$, with damping ratios more or less comprised between $2 - 4\%$ (note that a 0.2% damping ratio was considered for the untreated beam). Furthermore, it should be noted that the values of the natural frequencies remain practically the same for the different thicknesses, with values for the thickness $0.03\,\mathrm{mm}$ equal to $22.57\,\mathrm{Hz}$, $119.9\,\mathrm{Hz}$, $281.7\,\mathrm{Hz}$, $578.9\,\mathrm{Hz}$ and $1040\,\mathrm{Hz}$. Since the aims of the treatment are to attenuate significantly the first 5 modes, and since a trade off in modal damping performance occurs for different thicknesses, the optimal thickness value was set to $0.03\,\mathrm{mm}$, revealing the effects of the passive piezoelectric (without control) treatment. That is the thickness value optimized for the PCLD treatment utilized herein.

With the optimal thickness chosen, the next step is to actively utilize the piezoelectric layers, through connection with the LQG controller, to enhance the PCLD treatment performance. Here, a SISO control system is considered with the input being the control voltage applied into the piezoelectric layers, which since the treatment is symmetrically collocated is the same for both active layers but with opposite polarity, and the output being the velocity of the free tip of the beam, which is assumed to be measured. In order to damp the first five modes, and since they occur in complex conjugated pairs, the LQR state weighting matrix for the real equivalent system, as pointed out in Section 3.1, is set to $\mathbf{Q}_x = 1 \times 10^6 \mathrm{diag}(\omega_1^2, \omega_1^2, \ldots, \omega_5^2, \omega_5^2, 0, \ldots, 0)$ and the control input weighting matrix to $\mathbf{R} = 1$. For the LQG controller design, a white noise mechanical disturbance applied on the free end of the beam is modeled as plant noise. Therefore, the equality $\mathbf{B}_w = \mathbf{B}_u$ in Equation (30) should be considered, and a plant noise vector (force disturbance) with $E[\mathbf{w}(t)\mathbf{w}^{\mathrm{T}}(t)] = 0.25\,\mathrm{N}^2$ and a sensor white noise disturbance with $E[\mathbf{v}(t)\mathbf{v}^{\mathrm{T}}(t)] = 1 \times 10^{-5}\,\mathrm{V}^2$ are considered for the definition of the noise correlation

matrices and Kalman-Bucy gain design. It should be mentioned that the only output measured considered in the Kalman filter estimation is the velocity at the free tip. Furthermore, in order to avoid the depolarization of the piezoelectric actuators, the maximum control voltage applied is set to $250\,\mathrm{V}$, leading to a maximum electric field of $250\,\mathrm{V}/\,\mathrm{mm}$.

The control voltage and time displacement at the free end, for a white noise mechanical force disturbance applied at the free end too, for the bare beam and PCLD and ACLD treated beam configurations are obtained with Simulink®, with the sampling frequency set to $10000\,\mathrm{Hz}$, and are presented in Figure 6. It can be seen that both the PCLD and ACLD treatments manage to reduce the tip displacement significantly. When compared to the bare beam displacement standard deviation, which is equal to $5.9\,\mathrm{mm}$, the standard deviations of the PCLD and ACLD treatment cases, which is equal to $1.59\,\mathrm{mm}$ and $0.76\,\mathrm{mm}$, respectively, demonstrate the vibration control efficiency. Moreover, it can be seen that when compared with the fail safe PCLD treatment, the ACLD treatment improves even further (around 50%) the damping performance, with the actuating control voltage not exceeding $250\,\mathrm{V}$.

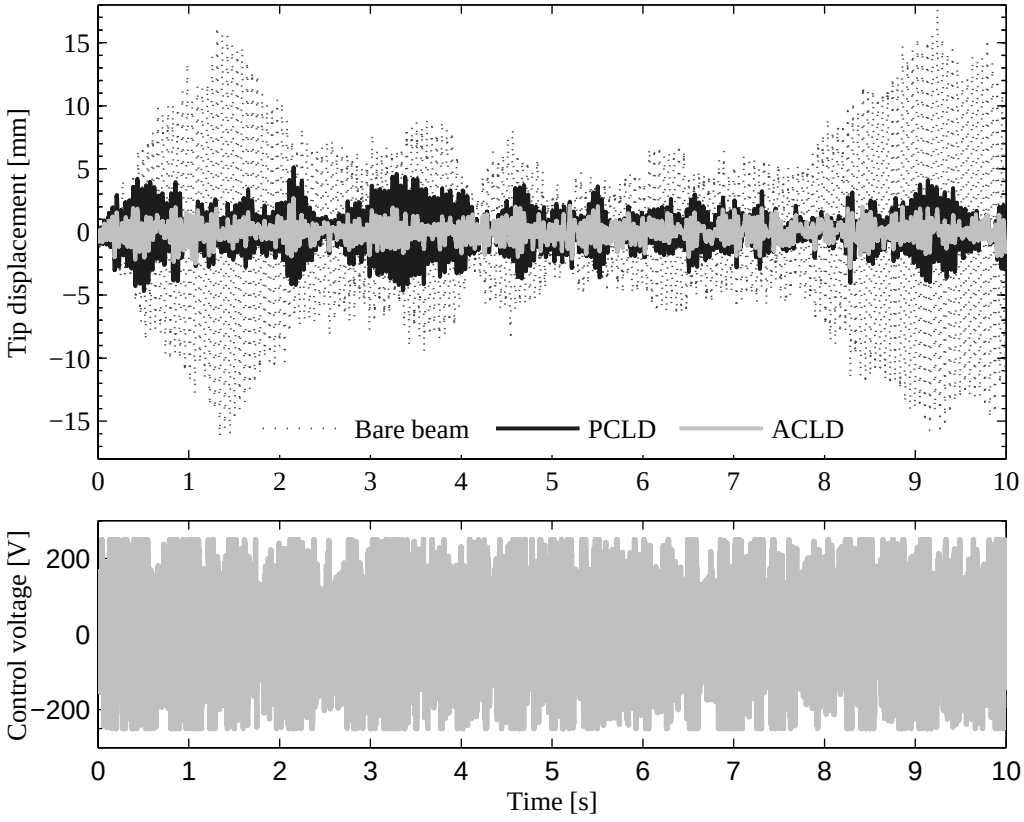

Figure 6. Control voltage and tip displacement histories at the free tip for a white noise mechanical force disturbance applied at the free end of the beam for the bare beam, PCLD and ACLD treatment configurations.

In order to analyze the capacity of the PCLD and ACLD treatments in the frequency domain,

the point receptances at the free end of the beam are presented in Figure 7. The PCLD treatment significantly reduces the magnitude of the first resonance in approximately 7 dB and the ACLD treatment in approximately 20 dB. Furthermore, the PCLD manages to significantly attenuate all modes; in comparison the ACLD attenuates them even more, except the third mode which rests almost unaltered, and the fifth is completely eliminated. Moreover, the damping ratios of the first five modes obtained with PCLD are 2.20%, 2.46%, 1.74%, 2.88%, 3.65% and with ACLD are 10%, 12%, 2.46%, 15.3%, 100%, which should be compared with the 0.2% for all modes obtained for the bare beam. Both Figures 6 and 7 show the adaptability and improvement in the damping capabilities obtained with the ACLD treatment, and the robustness and highly satisfactory performance of the PCLD in case the active system controller fails, when the beam is under stochastic mechanical disturbances.

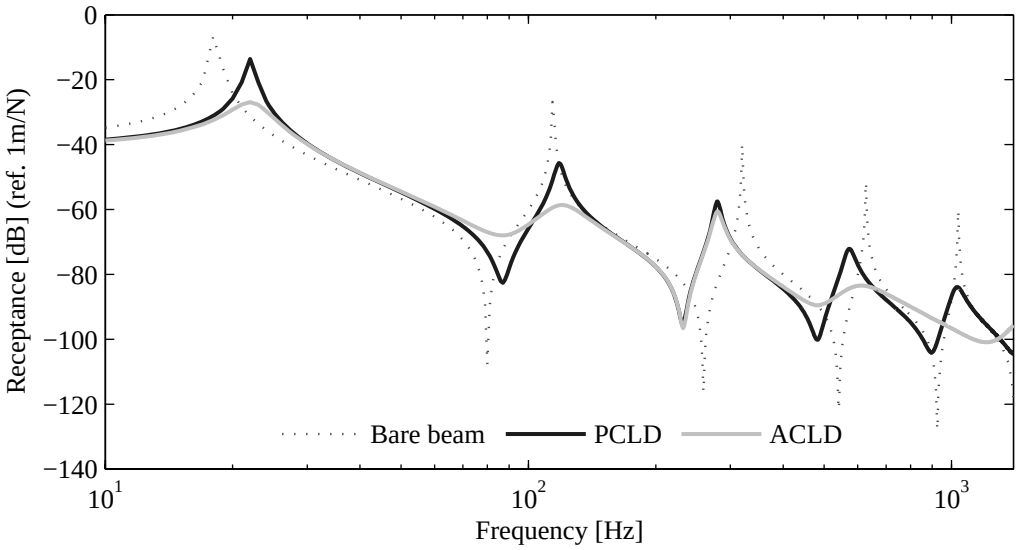

Figure 7. Point receptance at the free tip for the bare beam, PCLD and ACLD treatment configurations.

In order to attenuate the effects of a sinusoidal point-force disturbance oscillating at a frequency of $600\,\mathrm{Hz}$, the well known adaptive filtered-reference LMS algorithm is utilized. First, the LMS algorithm is used to identify the plant cancellation path (control voltage to measured velocity path) at the disturbance frequency, which for a single frequency only requires to filter weights, with the convergence being achieved in nearly $0.5\,\mathrm{s}$. After identifying the plant along the cancellation path, the filtered-reference LMS algorithm was implemented. Again, only two filter weights were considered in the adaptive feedforward controller and the results are presented in Figure 8. As can be seen, the control voltage is limited to $250\,\mathrm{V}$ in absolute value, and the ACLD feedforward controller manages to reduce the free tip displacement significantly when compared with the PCLD one. Furthermore, the filter weights did not converge yet at the time of $5\,\mathrm{s}$.

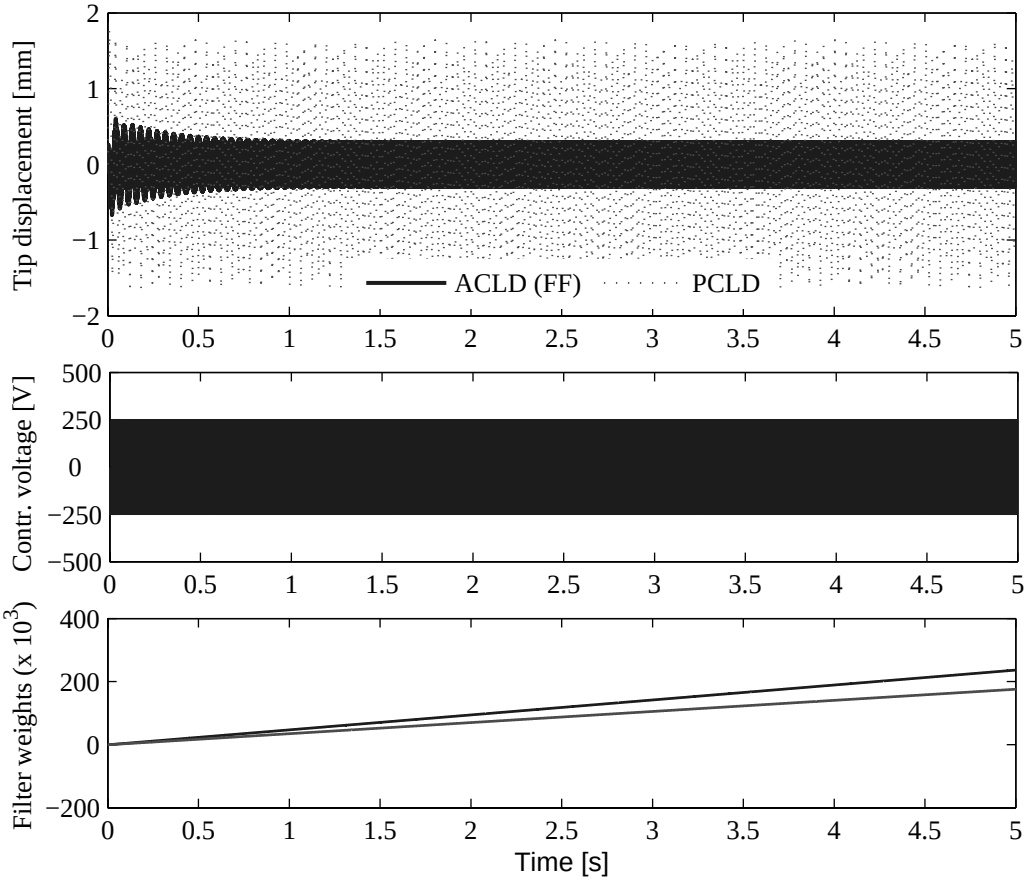

Figure 8. Tip displacement, control voltage and filter weights, for a sinusoidal disturbance applied at the free end of the beam, obtained with the adaptive feedforward controller for the PCLD and ACLD treatment configurations.

While the filtered-reference LMS algorithm can be used to successfully control a periodic disturbance, as shown in Figure 8, feedback control is often more appropriate for control of stochastic disturbances. This is particularly true when an uncontrollable reference signal can not be identified and the system is subject to both periodic and stochastic disturbances. To demonstrate the complimentary performance of the two control approaches, the hybrid control approach described in Section 3.3 is implemented for the same sinusoidal disturbance. The same SISO system in the previous example is used here; however, the LQG dynamic compensator designed earlier for the stochastic disturbances is also incorporated in the control path, which modifies the plant that is acted on by the feedforward controller. Therefore, the modified cancellation path is identified again. The results of the hybrid controller are presented in Figure 9.

As can be seen from the analysis of Figures 8 and 9, when the hybrid control system is engaged, linearly combining both feedback and adaptive feedforward, and for the same convergence parameter, the displacement converges faster. The displacement results are plotted on the

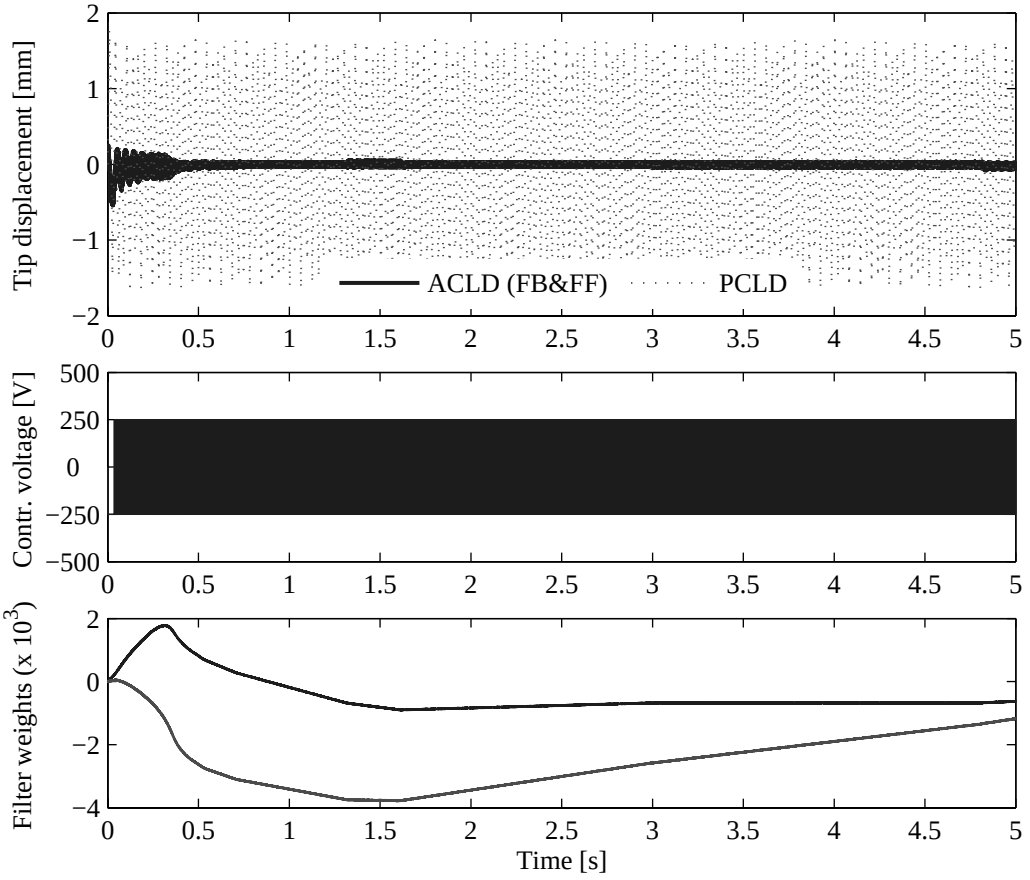

Figure 9. Tip displacement, control voltage and filter weights, for a sinusoidal disturbance applied at the free end of the beam, obtained with the adaptive hybrid controller for the PCLD and ACLD treatment configurations.

same scale to display the improved convergence characteristics and transient response performance. Furthermore, at the end of the period of time considered in the simulation ($t = 5\,\mathrm{s}$), the displacement with the adaptive feedforward controller is comprised in an interval of amplitude $0.3\,\mathrm{mm}$ while with the hybrid controller a $0.05\,\mathrm{mm}$ amplitude was obtained. These values are obtained for the ACLD case and when compared with the results of the PCLD system, $2\,\mathrm{mm}$ amplitude, demonstrate the effectiveness of the ACLD treatment. Moreover, note that there is an initial transient response of the structure when the sinusoidal disturbance is introduced at $t = 0\,\mathrm{s}$. This transient response decays much faster with the hybrid controller and converges to a lower displacement amplitude value.

5 CONCLUSION

In this paper a generic formulation for the study of beams with arbitrary active constrained layer damping (ACLD) treatments was presented. A finite element (FE) model, considering a partial layerwise displacement formulation and a fully coupled electromechanical theory, was

succinctly presented and utilized to model the structural system. The damping behavior of the viscoelastic layers was considered by a Laplace transformed *Anelastic Displacement Fields* (ADF) method and implemented in the FE model. Furthermore, the optimal feedback, *Linear Quadratic Gaussian* (LQG), and adaptive feedforward, *filtered-reference LMS,* controllers were described and discussed when used individually or combined in a unified hybrid controller.

The analyzed case study regards the disturbance rejection of an aluminium beam with a pair of symmetrically collocated surface mounted ACLD patches. For the design and simulation of the control system, Matlab® and Simulink® softwares were utilized, and a single-input single-output (SISO) configuration, with the output being the velocity at the free end of the beam, and the input being the control voltage applied into the piezoelectric constraining layers, was considered. First, a broadband stochastic disturbance was considered and a feedback controller was utilized to suppress vibration. Then, considering that the designer has access to a periodic reference signal that is correlated with the disturbance, an adaptive feedforward strategy was employed to cancel the effects of the disturbance on the plant. Finally, both controllers were combined into a unified hybrid controller.

The case study allowed to assess and discuss the outcomes and drawbacks of the feedback and feedforward controllers when used individually and the advantages of the hybrid controller. The hybrid controller improved the feedback performance and led to an improved performance and convergence of the adaptive feedforward controller. The transient response of the adaptive hybrid control system was observed to converge on a much faster timescale due to the modification of the system dynamics resulting from the feedback control. The rate of convergence for the adaptive controller is thus increased in hybrid configurations.

ACKNOWLEDGEMENTS

The authors wish to gratefully acknowledge the funding given by *Fundação para a Ciência e a Tecnologia* of the *Ministério da Ciência e da Tecnologia* of Portugal under grant POSI SFRH/BD/13255/2003.

REFERENCES

[1] A. Baz. Active constrained layer damping. In *Proceedings of Damping' 93*, volume 3, pages IBB 1–23, San Francisco, CA, 1993.

[2] C. H. Park and A. Baz. Vibration damping and control using active constrained layer damping: A survey. *The Shock and Vibration Digest*, 31(5):355–364, 1999.

[3] A. Benjeddou. Advances in hybrid active-passive vibration and noise control via piezoelectric and viscoelastic constrained layer treatments. *Journal of Vibration and Control*, 7(4):565–602, 2001.

[4] R. Stanway, J. A. Rongong and N. D. Sims. Active constrained-layer damping: A state-of-the-art review. *Proceedings of the Institution of Mechanical Engineers. Part I: Journal of Systems and Control Engineering*, 217(6):437–456, 2003.

[5] L. Meirovitch. *Dynamics and Control of Structures*. John Wiley & Sons, New York, 1990.

[6] C. R. Fuller, S. J. Elliott and P. A. Nelson. *Active Control of Vibration*. Academic Press, London, 1996.

[7] R. L. Clark, W. R. Saunders and G. P. Gibbs. *Adaptive Structures: Dynamics and Control*. John Wiley & Sons, New York, 1998.

[8] C. H. Hansen and S. D. Snyder. *Active control of noise and vibration*. E & FN Spon, London, 1997.

[9] S. J. Elliott. *Signal processing for active control*. Signal processing and its applications. Academic Press, San Diego, CA, 2001.

[10] R. Alkhatib and M. F. Golnaraghi. Active structural vibration control: A review. *Shock and Vibration Digest*, 35(5):367–383, 2003.

[11] S. Poh, A. Baz and B. Balachandran. Experimental adaptive control of sound radiation from a panel into an acoustic cavity using active constrained layer damping. *Smart Materials and Structures*, 5(5):649–659, 1996.

[12] H. Illaire. *A study of active-passive damping treatments*. Ph.D. Thesis, Department of Applied Acoustics, Chalmers University of Technology, 2004.

[13] C. M. A. Vasques, B. Mace, P. Gardonio and J. D. Rodrigues. Analytical formulation and finite element modelling of beams with arbitrary active constrained layer damping treatments. *Institute of Sound and Vibration Research*, Technical Memorandum TM934, 2004.

[14] C. M. A. Vasques, B. R. Mace, P. Gardonio and J. D. Rodrigues. Arbitrary active constrained layer damping treatments on beams: Finite element modelling and experimental validation. *Computers and Structures*, 2005 (in press).

[15] J. F. Nye. *Physical Properties of Crystals: Their Representation by Tensors and Matrices*. Clarendon Press, Oxford, 1957.

[16] The Institute of Electrical and Electronics Engineers Inc. *IEEE Standard on Piezoelectricity*. ANSI/IEEE Std 176-1987, 1988.

[17] M. Krommer and H. Irschik. On the influence of the electric field on free transverse vibrations of smart beams. *Smart Materials and Structures*, 8(3):401–410, 1999.

[18] C. M. A. Vasques and J. D. Rodrigues. Coupled three-layered analysis of smart piezoelectric beams with different electric boundary conditions. *International Journal for Numerical Methods in Engineering*, 62(11):1488–1518, 2005.

[19] H. F. Tiersten. *Linear Piezoelectric Plate Vibrations*. Plenum Press, New York, 1969.

[20] J. N. Reddy. *An introduction to the finite element method*. McGraw-Hill, New York, 1984.

[21] C. M. A. Vasques. *Modelização do Controlo Activo de Vibrações de Vigas com Sensores e Actuadores Piezoeléctricos*. M.Sc. Thesis, Faculty of Engineering, University of Porto, Porto, Portugal, 2003 (in Portuguese).

[22] G. A. Lesieutre and E. Bianchini. Time domain modeling of linear viscoelasticity using anelastic displacement fields. *Journal of Vibration and Acoustics*, 117(4):424–430, 1995.

[23] G. A. Lesieutre, E. Bianchini and A. Maiani. Finite element modeling of one-dimensional viscoelastic structures using anelastic displacement fields. *Journal of Guidance Control and Dynamics*, 19(3):520–527, 1996.

[24] R. M. Christensen. *Theory of Viscoelasticity: An Introduction*. Academic Press, New York, 2nd edition, 1982.

[25] A. Nashif, D. Jones and J. Henderson. *Vibration Damping*. John Wiley & Sons, New York, 1985.

[26] D. I. G. Jones. *Handbook of Viscoelastic Vibration Damping*. John Wiley & Sons, Chichester, 2001.

[27] G. A. Lesieutre. Finite elements for dynamic modeling of uniaxial rods with frequency dependent material properties. *International Journal of Solids and Structures*, 29(12):1567–1579, 1992.

[28] G. A. Lesieutre and U. Lee. A finite element for beams having segmented active constrained layers with frequency-dependent viscoelastics. *Smart Materials and Structures*, 5(5):615–127, 1996.

[29] M. A. Trindade, A. Benjeddou and R. Ohayon. Modeling of frequency-dependent viscoelastic materials for active-passive vibration damping. *Journal of Vibration and Acoustics*, 122(2):169–174, 2000.

[30] J. B. Burl. *Linear Optimal Control*. Addison-Wesley, California, 1999.

[31] H. Kwakernaak and R. Sivan. *Linear optimal control systems*. John Wiley & Sons, New York, 1972.

[32] M. J. Balas. Feedback control of flexible systems. *IEEE Transactions on Automatic Control*, AC-23(4):673–679, 1978.

[33] M. J. Lam, D. J. Inman and W. R. Saunders. Hybrid damping models using the golla-hughes-mctavish method with internally balanced model reduction and output feedback. *Smart Materials and Structures*, 9(3):362, 2000.

[34] R. Bouc and E. Friot. Contrôle optimal par retroaction du rayonnement d'une plaque munie de capteurs et d'actionneurs piézo-électriques non colocalisés. In *2eme Colloque GDR Vibroacoustique*, pages 229–248, Marseille, 1996.

[35] C. M. A. Vasques and J. D. Rodrigues. Active vibration control of smart piezoelectric beams: Comparison of classical and optimal feedback control strategies. *Computers and Structures*, 2005 (in press).

[36] B. Widrow and S. D. Stearns. *Adaptive signal processing*. Prentice-Hall, Englewood Cliffs, 1985.

[37] S. S. Haykin. *Adaptive filter theory*. Prentice Hall, Upper Saddle River, NJ, 4th edition, 2001.

[38] 3M. *Scotchdamp Vibration Control Systems: Product Information and Performance Data*. 3M Industrial Tape and Specialties Division, St. Paul, 1993.